Geophys. J. Int. (2006) **165,** 775–785 doi: 10.1111/j.1365-246X.2006.02951.x

The role of magnetostatic interactions in sediment suspensions

D. Heslop,[1] A. Witt,[1] T. Kleiner[1,2] and K. Fabian[1]

[1]*Department of Geosciences, University of Bremen,* PO Box 330 440, 28344 *Bremen, Germany. E-mail: dheslop@uni-bremen.de*
[2]*Department of Geosciences, University of Münster, Robert-Koch Str.* 26-28, 48149 *Münster, Germany*

Accepted 2006 February 3. Received 2005 December 2; in original form 2005 March 21

SUMMARY

The processes that influence a detrital remanent magnetization as well as the physical microscale factors that control formation of a stable post-depositional remanent magnetization are still not fully understood. Previous laboratory studies and statistical numerical approaches have shown the possibility that sediment suspensions can display complex magnetization phenomena. Such behaviour has been attributed to the effect of magnetostatic interactions in the suspension, which could provide one explanation for spurious magnetizations observed in marine sediment cores. In laboratory experiments we investigated magnetization decay as a function of time in sediment suspensions produced with varying lithologies and particle concentrations. A companion model takes into account the physics of magnetic particle–particle interactions, Brownian motion and hydrodynamic forces to investigate numerically the magnetization behaviour of sediment suspensions. When combined, the experiments and the numerical models reveal a weak effect of magnetostatic interactions in the natural sediment suspensions, which is expressed as an increase in the magnetization decay rate. In addition, a calculation of effective particle size based on the response of each suspension to Brownian motion indicates that the majority of the sedimentary magnetic particles are attached to larger clay particles.

Key words: depositional remanent magnetization, magnetostatic interaction, suspension.

1 INTRODUCTION

Reconstruction of the Earth's palaeofield based on the measurement of detrital remanent magnetizations (DRM) recorded in sedimentary archives is a well-established technique (Verosub 1977; Tauxe 1993; Valet 2003). Identification of specific features within these records, such as geomagnetic reversals and excursions, provide a basis upon which stratigraphic frameworks and chronologies can be constructed. In addition, the continuous nature of sedimentary records makes them suitable for providing constraints on expected field behaviour for geodynamo models (Dormy *et al.* 2000; Kono & Roberts 2002).

The general picture of DRM formation involves the rotation of magnetic sediment particles in response to the torque they experience from the Earth's magnetic field as they descend through the water column. Calculations by Collinson (1965) and Stacey (1972) demonstrated that for typical geomagnetic field conditions, the imposed torque would rapidly bring individual magnetic particles into alignment with the ambient field direction. A number of disordering processes do, however, act on the settling particles and even during descent through calm water the alignment of an assemblage of particles will have a distribution of orientations. Small particles will be strongly influenced by Brownian motion and will undergo both translational displacement and rotational motion due to bombardment by the water molecules that surround them. Previous calculations (Collinson 1965; Stacey 1972) have shown that the effects of Brownian motion have a primary importance on the alignment of the magnetic particles and, thus, on the final DRM. Because Brownian motion is a random process, the probability of a particle being subjected to a torque acting in an anticlockwise manner is equal to that of one acting in a clockwise manner. Therefore, for large assemblages of particles the magnitude of the DRM will be reduced by the disordering effects of Brownian motion but the direction of the overall magnetization should remain aligned with the external field.

Once a particle reaches the sediment–water interface, its orientation will be influenced by a number of different processes (Verosub 1977). Gravitational torques will act on elongated particles, attempting to align them horizontally (Griffiths *et al.* 1960; King & Rees 1966). Motion of the water at the sediment surface will produce hydrodynamic torques that, in the case of persistent currents, will tend to align the magnetic particles in a preferred direction and, in the case of turbulent flow, will act as a disordering mechanism (Griffiths *et al.* 1960; Rees 1961). Bioturbation will result in a reorientation of the magnetic particles as the activities of various organisms restructure the sedimentary fabric. Irving & Major (1964) proposed that as compaction of the deposited sediment proceeds and porosity is reduced the magnetic grains will be gradually locked into a set orientation that forms the stable DRM. Because this signal is formed below the sediment–water interface it is termed a post-depositional remanent magnetization

(PDRM). A number of processes that will both order and disorder the orientation of the magnetic particles to form a final DRM have been identified, and both theoretical (Shcherbakov & Shcherbakova 1983, 1987; Katari & Bloxham 2001) and experimental approaches (Anson & Kodama 1987; Barton *et al.* 1980; Kent 1973; Løvlie 1989; Lu *et al.* 1990; Tauxe & Kent 1984; van Vreumingen 1993a,b) have been adopted to investigate the relative importance and the interaction between the different processes. On the basis of the above work and the successful recovery of palaeomagnetic records from the oceanic realm, it is generally accepted that the DRM vector in marine sediments is at least partially a function of the geomagnetic-field conditions during deposition.

Compilations of sedimentary palaeomagnetic data sets provide evidence that during the Brunhes normal polarity chron, 10 or more geomagnetic excursions may have occurred (Langereis *et al.* 1997; Guyodo *et al.* 2000). In a large number of reported records, however, these geomagnetic features are found to be absent. If it is assumed that geomagnetic excursions are global (Guyodo *et al.* 2000; Valet *et al.* 2005) then it must be concluded that not all sedimentary archives are of a sufficiently high enough fidelity to provide a comprehensive history of geomagnetic variation (Roberts & Winklhofer 2004). In the light of this evidence a number of processes that could lead to inaccurate sedimentary recording of the field have been proposed.

Of specific interest here is the work of Yoshida & Katsura (1985) who investigated the magnetic relaxation behaviour of dilute suspensions of clays and limey mud. The individual suspensions were exposed to a weak external field in an attempt to orientate all of the magnetic particles in a single direction. Upon removal of the external field the decay in magnetization of the suspensions could be measured as a function of time to characterize the process of relaxation by particle reorientation. Based on the shape of the magnetization decay curves, Yoshida & Katsura (1985) defined three *classes* of relaxation behaviour. The relaxation pattern of suspensions of both reddish brown clay and calcareous ooze with concentrations $\geq 0.1\,\mathrm{g\,ml^{-1}}$ displayed nearly no decay in magnetization (Fig. 1, *Class 1*). The stable *Class 1* magnetization was attributed to flocculation of the sediment particles that formed an ordered fabric and restricted the motion of the magnetic particles. This explanation is supported by Shcherbakov & Shcherbakova (1987) who showed that suspensions with such high concentrations should be considered as slurries possessing elasticity, viscosity and plasticity due to the formation of coagulated structures by particle cohesion. The properties of dilute slurries are expected to substantially reduce grain mobility (Shcherbakov & Shcherbakova 1987) and, therefore, inhibit strongly the randomization of particle orientations due to Brownian motion.

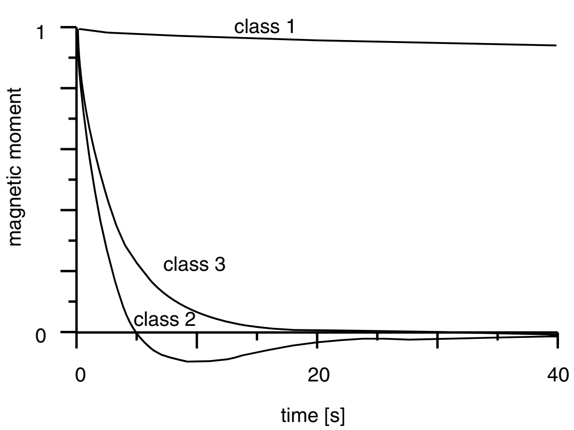

Figure 1. Experimental results of Yoshida & Katsura (1985), using a sediment suspension consisting mainly of reddish-brown clay, show three different classes of magnetic relaxation pattern. *Class 1* and *Class 2* are attributed to electrostatic and magnetostatic interactions within the sediment suspension, respectively. *Class 3* is thought to represent a non-interacting system that is dominated by Brownian motion.

Suspensions with intermediate particle concentrations (0.1–$0.004\,\mathrm{g\,ml^{-1}}$ in the reddish brown clay and 0.1–$0.01\,\mathrm{g\,ml^{-1}}$ in the calcareous ooze) displayed an exponential decay of magnetization followed by a polarity change before approaching zero (Fig. 1, *Class 2*). This behaviour was found to be reproducible and the magnitude of the polarity change increased with increasing particle concentration. Due to the concentration dependency of the pattern, the observed behaviour was attributed to the effect of magnetostatic interactions within the sediment suspension. Yoshida & Katsura (1985) gave no clear explanation of how the clumping of magnetic particles due to magnetostatic interaction could result in polarity changes during relaxation, but suggested that inertial rotation of flocced grains could play a key role.

The suspension with the lowest particle concentration ($<0.004\,\mathrm{g\,ml^{-1}}$ in the reddish brown clay and $<0.01\,\mathrm{g\,ml^{-1}}$ in the calcareous ooze) displayed an exponential decay of magnetization (Fig. 1, *Class 3*) that was attributed to a non-interacting system dominated by Brownian motion. In this case, the *Class 2* type relaxation behaviour provides a mechanism that could possibly explain the formation of spurious magnetization records in weak field conditions.

Fukuma (1992) performed a numerical simulation of magnetic particle coagulation in a fluid using a Monte Carlo procedure. It was found that for simulated suspensions with a sufficiently high concentration of particles, magnetostatic interactions could result in relaxation curves with a switch in polarity similar to the *Class 2* curves of Yoshida & Katsura (1985). Magnetic particle concentrations >10 ppm were required to produce a switch in polarity during relaxation, however, this concentration cannot be considered as realistic because the model did not take into account the presence of non-magnetic particles and coagulation mechanisms such as van der Waals forces.

It is known from laboratory redeposition experiments that the form of the non-magnetic sedimentary matrix and its interaction with the magnetic mineral assemblage plays an important role in DRM formation. DRM intensity is thought to be partially controlled by pH and electrolyte content indicating that flocculation of the sediment grains plays a role in the formation of the palaeomagnetic signal (Lu *et al.* 1990; Katari & Tauxe 2000). Katari & Tauxe (2000) produced an interesting hypothesis that isolated magnetite particles do not occur in sediment suspensions, but instead, due to interparticle forces, magnetite particles will generally be attached to clay particles and it is these units that must be rotated to form a DRM.

Magnetostatic interactions occur in some natural sediments and could, therefore, play an important role in the process of DRM acquisition. It is, however, a difficult task to relate the magnitude of interactions in a compacted sediment sample to those present in a suspension. For example, although first-order reversal curve (FORC) data (Roberts *et al.* 2000) show interaction between single domain particles in sediments it is known that a number of the samples contain minerals formed post-depositionally, for example, strongly interacting clusters of authigenic greigite (Roberts & Weaver 2005).

To investigate the influence of magnetostatic interactions, we present laboratory studies of magnetization decay in sediment suspensions accompanied by a numerical model representing interacting magnetic particles in water. The model takes into account the physical theory of interacting magnetic particles, hydrodynamic forces and Brownian motion. While we investigate behaviour in the water column, sediment fabrics near the sediment–water interface are highly porous (Kranck 1991; Wartel *et al.* 1991; Bennett *et al.* 1991) and, therefore, the processes that control the magnetic behaviour of a slurry could also be valid for such sediments.

2 EXPERIMENTS

2.1 Laboratory experiments

The experiments that were performed to investigate the role of magnetostatic interactions in sediment suspensions were designed to match the experiments of Yoshida & Katsura (1985). Measurements of magnetization decay were performed in zero field in order to be able to define the influence of magnetostatic particle–particle interaction without bias due to an external field. For the presented experiments, 20 samples were taken from four different gravity cores recovered from the South Atlantic Ocean. The cores cover a broad range of lithologies (high biogenic opal content, carbonate rich and clayey sediment) with rock magnetic properties that have been discussed previously by Franke *et al.* (2004). The chosen samples all had a magnetic susceptibility greater than $300 \cdot 10^{-6}$ SI and their hysteresis properties (Fig. 2), suggest that the magnetic particles lie predominantly in the stable single-domain range (Tauxe *et al.* 2002).

To follow the procedure of Yoshida & Katsura (1985), the sediment samples were suspended in distilled water mixed with approximately 3 mg of surfactant ($Na_4P_2O_7 \cdot 10\,H_2O$). The surfactant will reduce electrostatic attraction at the particle surfaces, thus dispersing the sediment, but will have no influence on clumping due to magnetostatic interactions. This means that magnetic particles may be initially clumped together when the suspension is prepared. If this is the case then the interactions in the suspensions may be stronger than would be expected in natural suspensions of similar concentrations. Sieving was then performed to remove the sediment

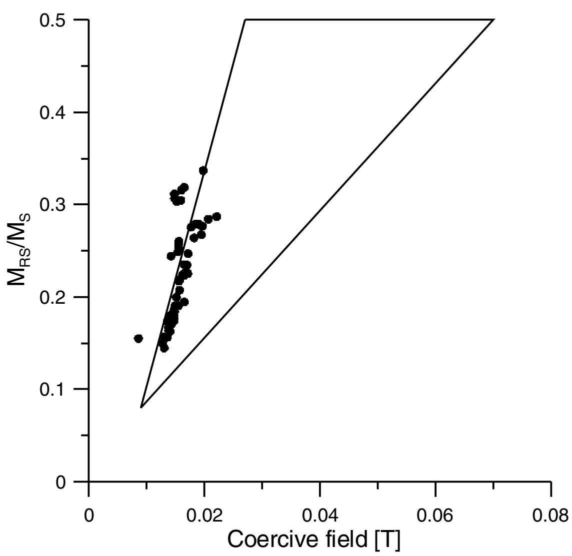

Figure 2. Ratio of saturation remanent magnetization to saturation magnetization (M_{RS}/M_S) plotted against the coercive field. According to Tauxe *et al.* (2002), data that plot within the triangle can be considered to represent mixtures of single domain magnetite particles and superparamagnetic material. The samples plot along the left edge of the triangle, which, according to Tauxe *et al.* (2002), corresponds to a mixture containing uniaxial single domain magnetite with a length to width ratio of 1.3.

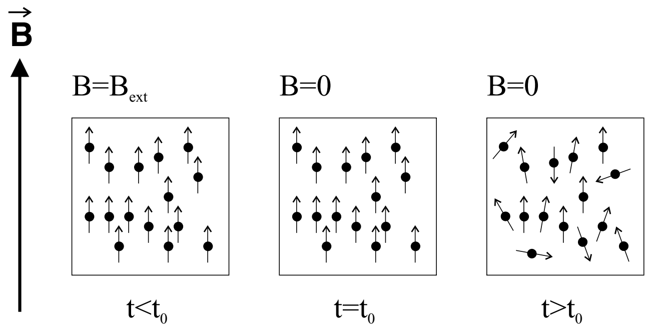

Figure 3. When a sediment suspension is exposed to a magnetic field for 30 s, the particles align with the external field. At time $t = t_0$, the field is switched off and measurement of the magnetization commences. The decay of magnetization is recorded as a function of time for 120 s.

fraction with diameters above 20 μm. The samples were homogenized by treatment in an ultrasonic bath and stirring. The sediment suspensions were concentrated by allowing the sediment to settle and by removing the excess water. Nine different samples with concentrations c_n were produced from each suspension ($c_n = 2^{-n}c_0$, $n = 0, \ldots, 8$ and $c_0 = 1.5 \cdot 10^{-1}\,\mathrm{g\,ml^{-1}}$) and placed in 6.2 cm^3 plastic cubes.

At the commencement of each experiment the suspension filled sample cubes were placed in an ultrasonic bath for 1 min in order to disperse the particles uniformly. The samples were then transported for 120 s in field-free conditions and placed in a 2G Enterprises cryogenic SQUID magnetometer. After being exposed to a 100 μT field along the sample z-direction for 30 s, the suspension magnetization was measured in zero field over a period of 120 s. The basic concept of the laboratory studies is shown in Fig. 3.

It is important to consider the relative scales of the time required for the orientation of a magnetic particle to be randomized by Brownian motion and the duration of the particle descent to the base of the sample cube. This balance can be important because in the case of a particle descending to the base of the cube in a period shorter than that required for randomization, some memory of the applied field will be retained. An estimate of the balance can be made by considering the simple model of an isolated sphere descending through water under the influence of gravity. Considering a collection of magnetic particles in an aligned starting state the system magnetization, M, will decay exponentially as a function of time, t, according to the relationship $M(t) = \exp(-t/\tau)$ (Debye 1929; Fannin *et al.* 1995). For suspensions with constant viscosity τ is independent of concentration and is given by:

$$\tau = \frac{3V\eta}{kT}, \qquad (1)$$

where V is the particle volume, η is the fluid viscosity, k is Boltzmann's constant and T is the absolute temperature. The terminal velocity, V_t, of a spherical particle is given by:

$$V_t = \frac{2R^2\rho}{9\eta} g \left(1 - \frac{\rho'}{\rho}\right), \qquad (2)$$

where R is the particle radius, ρ and ρ' are the densities of the particle and fluid, respectively, and g is the acceleration of free fall. By assuming that a particle of given diameter is travelling at terminal velocity it is possible to calculate the distance it will descend through the cube in time τ (Fig. 4). It is apparent that large particles ($> \sim 7\,\mu$m) will descend through the cube in a period shorter than τ. For smaller particles of typical single-domain magnetite sizes, for example, 100 nm the time required to descend through the cube

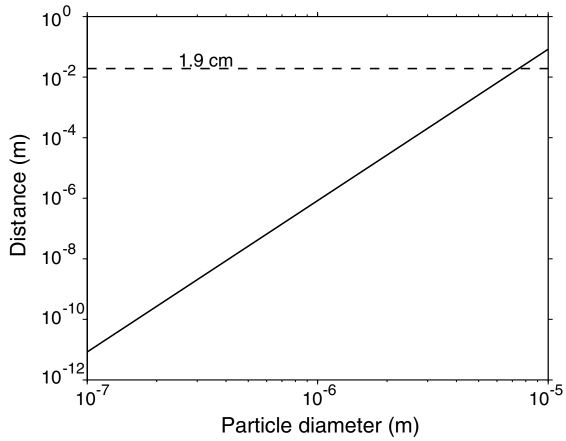

Figure 4. For sediment particles descending through the sample cube (∼1.9 cm in height) it is important to consider the relative magnitudes of the times required for descent and randomization by Brownian motion. By determining the distance travelled by a particle moving at terminal velocity in time τ it is clear that full randomization should occur for all but the very largest magnetic sediment particles.

is many orders of magnitude greater than τ. This simple approach does assume that the starting position of the particles is at the top of the cube, which will not be the case for a suspension subjected to an ultrasonic treatment. During the course of the settling, some particles will be deposited on the base of the sample cube. For particles that deposit rapidly it is also expected that they will preserve some memory of the applied field and thus form a depositional remanent magnetization.

2.2 Experimental results

Curves for a typical sediment sample provide an example of magnetization decay for suspensions c_0 to c_8 in Fig. 5. The suspension with the high sediment concentration (c_0) displays only a small decrease in magnetization with time. This behaviour is expected in the highest concentration suspensions, which will form slurries with reduced particle mobility (Shcherbakov & Shcherbakova 1987). If all the particles in suspension have an equal radius, then the decay of magnetization due to Brownian motion should be describable using a single exponential function. Our measurements do not meet this requirement and the magnetization as a function of time, m, normalized by its initial value can best be described using the sum of two exponential functions and a constant:

$$m(t) = a_1 e^{-a_2 t} + a_3 e^{-a_4 t} + a_5, \tag{3}$$

where $\tau_1 = 1/a_2$ and $\tau_2 = 1/a_4$ are the relaxation times of the respective exponentials. It is found that τ_1 and τ_2 generally decrease as concentration increases up to the second highest concentration, c_1 (Figs 6a and b). From the second highest to the highest concentration, there is a sharp increase in both τ_1 and τ_2. A Spearman rank correlation test showed that for 16 (τ_1) and 15 (τ_2) samples out of 20 there is a significant ($\alpha = 0.05$) monotonic decrease in τ_1 and τ_2 between c_8 and c_1. Plotting τ_1 against τ_2 reveals an approximately linear relationship between the two parameters (Fig. 6c).

Given the form of the curve in eq. (3), it is apparent that the dimensionless constant a_5 corresponds to a DRM formed as the particles settle on the base of the sample cube (Fig. 6d). Given that the experiment takes place in zero-field conditions, it must be inferred that if a_5 is non-zero then the deposited particles retain some memory of the initial 100 μT field treatment.

The viscosity of the suspensions is expected to increase with higher sediment concentration, therefore, according to eq. (1), the time required for relaxation of the magnetization due to rotational Brownian motion should increase with viscosity. The plots of τ_1 and τ_2 against concentration reveal a trend opposite to the expected behaviour, with the time required for relaxation decreasing with greater particle concentration. Increases in concentration are also expected to lead to increased flocculation and it is reasonable to assume that flocs will be more resistant to Brownian motion than the single particles from which they are composed. For our experiments, excluding the slurry samples, the rate of magnetization decay increases with increasing concentration. Therefore, the observed experimental behaviour cannot be explained by changes in the effectiveness of Brownian motion caused by concentration dependent viscosity and flocculation.

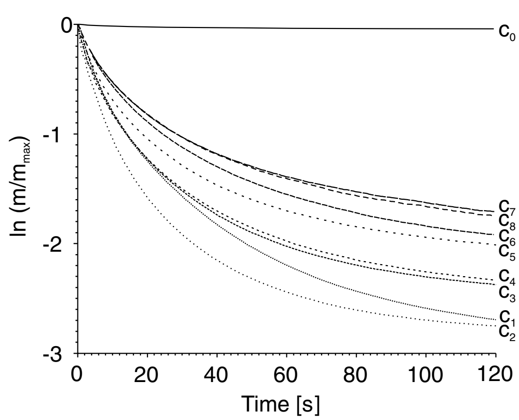

Figure 5. Experimental magnetic relaxation data for a typical sediment sample. The natural logarithm of the decay of nine different suspension concentrations is plotted against time. The highest concentration (c_0) acts as a slurry and shows only a small decrease in magnetization while the other suspensions relax far more quickly. If the decay curves were exponential then when plotted as the natural logarithm they would appear as straight lines. This is clearly not the case for the suspension samples.

3 NUMERICAL MODEL

3.1 Kinematics of magnetic particles in fluids

The experiments of Yoshida & Katsura (1985) raise the question of whether an interacting assemblage of remanence carriers in a fluid can exhibit a polarity switch as seen in the *Class 2* type curves (Fig. 1). To investigate this problem, the equations of motion of n magnetic particles with radii R_i and magnetic moments m_i in a fluid have to be solved. The *Class 2* effect observed by Yoshida & Katsura (1985) cannot be attributed to Brownian motion only, therefore, other processes must influence the relaxation behaviour of suspensions. Brownian motion, hydrodynamic forces and magnetic particle interaction are simulated in our numerical model. The particles are suspended in a carrier fluid of viscosity η and temperature T. The Reynolds number has a magnitude equal to approximately the square of the particle radius (Truckenbrodt 1980). Therefore, the inertia of the system is negligibly small (Truckenbrodt 1980), all inertial terms are zero and the motion of the particles is described by the equilibria of forces and torques.

$$\mathbf{F}_i^{\mathrm{mag}} + \mathbf{F}_i^{\mathrm{visc}} + \mathbf{F}_i^{\mathrm{brown}} = \mathbf{0}, \tag{4}$$

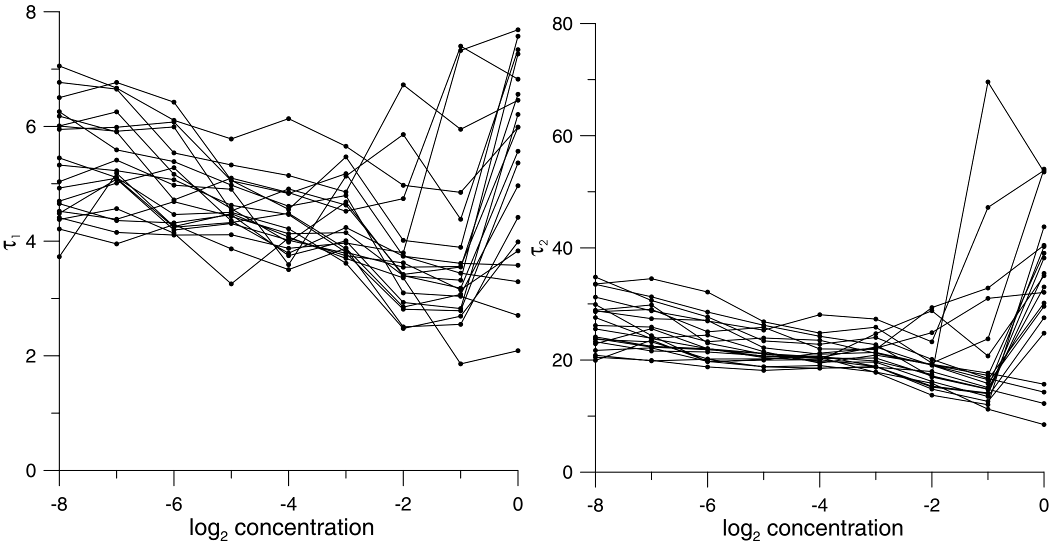

(a) (b)

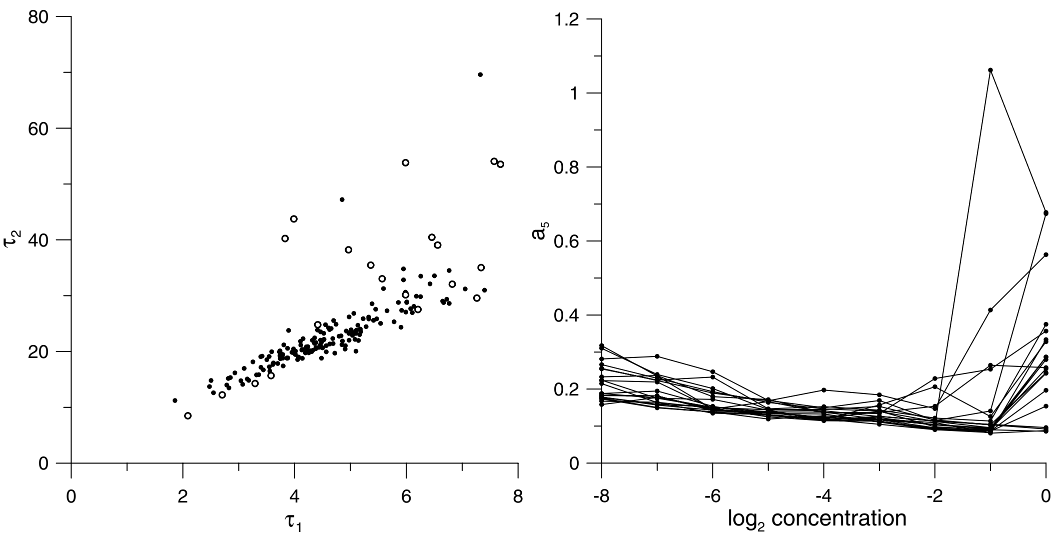

(c) (d)

Figure 6. (a) Relaxation time τ_1 plotted against a $\log_2$ based concentration. Out of 20 samples, 16 displayed a significant decrease in relaxation time moving from low to high concentrations and an increase in relaxation time moving from second highest to highest concentration. From left to right, the data points represent concentrations c_8 through to c_0. (b) Relaxation time τ_2 plotted against a $\log_2$ based concentration. Out of 20 samples, 15 displayed a significant decrease in relaxation time moving from low to high concentrations and an increase in relaxation time moving from second highest to highest concentration. (c) Relaxation time τ_1 plotted against relaxation time τ_2 The samples display an apparently linear relationship between τ_1 and τ_2 The majority of samples that do not follow the trend correspond to the highest concentration suspensions that show little decrease in magnetization (open symbols). (d) Constant a_5 plotted against a $\log_2$ based concentration. There is a sharp increase in a_5 moving from the second highest (c_1) to the highest (c_0) concentration. This increase can be attributed to increased flocculation of magnetic and non-magnetic particles resulting in locking of the magnetic particles.

$$\mathbf{L}_i^{\mathrm{mag}} + \mathbf{L}_i^{\mathrm{visc}} + \mathbf{L}_i^{\mathrm{brown}} = \mathbf{0}. \tag{5}$$

$\mathbf{F}_i^{\mathrm{mag}}$ and $\mathbf{L}_i^{\mathrm{mag}}$ are the force and torque exerted by the magnetic induction, $\mathbf{F}_i^{\mathrm{visc}}$ and $\mathbf{L}_i^{\mathrm{visc}}$ are the force and torque imposed by the fluid's viscosity and $\mathbf{F}_i^{\mathrm{brown}}$ and $\mathbf{L}_i^{\mathrm{brown}}$ are the force and torque attributed to Brownian motion, respectively. The latter will be accounted for by adding a random disturbance to the particle motion and will be discussed below. For all the models the fluid viscosity was assumed to be that of pure water (0.001 Pa s) and is, therefore, independent of suspension concentration.

3.2 Equations of motion

The forces that contribute to the motion of the particle i with position $\mathbf{r}_i$ are the force exerted by the viscous fluid, $\mathbf{F}_i^{\mathrm{visc}}$, and the force exerted by the magnetic field, $\mathbf{F}_i^{\mathrm{mag}}$. The latter depends on the magnetostatic self-energy E_i^{mag} of the ith dipole and the external magnetic field:

$$\mathbf{F}_i^{\mathrm{mag}} = -\nabla E_i(\mathbf{r}_i) \quad \text{and,} \tag{6}$$

$$E_i^{\mathrm{mag}}(\mathbf{r}_i) = -\mathbf{m}_i \cdot \mathbf{B}(\mathbf{r}_i), \quad \text{respectively.} \tag{7}$$

The magnetic induction $\mathbf{B}(\mathbf{r}_i)$ is, in the absence of an external magnetic field, the sum of the dipolar interaction fields:

$$\mathbf{B}(\mathbf{r}) = \frac{\mu_0}{4\pi}\sum_{i=1}^{n}\left(3\frac{(\mathbf{m}_i\cdot(\mathbf{r}-\mathbf{r}_i))(\mathbf{r}-\mathbf{r}_i)}{|\mathbf{r}-\mathbf{r}_i|^5} - \frac{\mathbf{m}_i}{|\mathbf{r}-\mathbf{r}_i|^3}\right). \tag{8}$$

The viscous fluid exerts a force opposite to the velocity of the dipole (Stoke's Law):

$$\mathbf{F}_i^{\mathrm{visc}} = -6\pi\eta R_i\dot{\mathbf{r}}_i. \tag{9}$$

This leads to the following equation of motion for particle translation:

$$\nabla(\mathbf{m_i}\cdot\mathbf{B}(\mathbf{r}_i)) = 6\pi\eta R_i\dot{\mathbf{r}}_i, \tag{10}$$

$$\Rightarrow \dot{\mathbf{r}}_i = \frac{1}{6\pi\eta R_i}\nabla(\mathbf{m_i}\cdot\mathbf{B}(\mathbf{r}_i)). \tag{11}$$

The terms contributing to the equilibria of torques are the torque attributed to the magnetic field, $\mathbf{L}_i^{\mathrm{mag}}$, and the torque attributed to the viscous fluid, $\mathbf{L}_i^{\mathrm{visc}}$. The magnetic field exerts a torque $\mathbf{L}^{\mathrm{mag}}$ acting on the dipoles (Gerthsen & Vogel 1993):

$$\mathbf{L_i}^{\mathrm{mag}} = \mathbf{m}_i\times\mathbf{B}(\mathbf{r}_i). \tag{12}$$

The rotation of the dipoles due to the magnetic field acts against the viscous fluid. The fluid's viscosity gives rise to a torque $\mathbf{L}^{\mathrm{visc}}$ which acts against $\mathbf{L}^{\mathrm{mag}}$. Assuming the particles to be of spherical shape, $\mathbf{L}^{\mathrm{visc}}$ takes on the following form (Currie 2002):

$$\mathbf{L_i}^{\mathrm{visc}} = -8\pi R_i^3\eta\dot{\varphi}, \tag{13}$$

where $\dot{\varphi}$ is the angular velocity of the particle. This leads to the following equation of motion:

$$\begin{aligned}
&\mathbf{m}_i\times\mathbf{B}(\mathbf{r_i}) = 8\pi R_i^3\eta\dot{\varphi}_i\\
&\Rightarrow \boldsymbol{\omega}_i = \dot{\varphi}_i = \frac{\mathbf{m}_i\times\mathbf{B}(\mathbf{r_i})}{8\pi R_i^3\eta}\\
&\Rightarrow \boldsymbol{\omega}_i\times\mathbf{e}_i = -\frac{1}{8\pi R_i^3\eta}\mathbf{e}_i\times(\mathbf{m}_i\times\mathbf{B}(\mathbf{r_i}))\\
&\Rightarrow \dot{\mathbf{e}}_i = \frac{-m_i}{8\pi R_i^3\eta}\mathbf{e}_i\times(\mathbf{e}_i\times\mathbf{B}(\mathbf{r_i}))\\
&\Rightarrow \dot{\mathbf{e}}_i = \frac{-m_i}{8\pi R_i^3\eta}(\mathbf{e}_i\cdot(\mathbf{e}_i\cdot\mathbf{B}(\mathbf{r_i})) - \mathbf{B}(\mathbf{r_i})),
\end{aligned} \tag{14}$$

where $m_i\mathbf{e}_i = \mathbf{m}_i$ and $|\mathbf{e}_i| = 1$, therefore $\mathbf{e}_i$ is a unit vector in the direction of $\mathbf{m}_i$.

3.3 Scaling

In order to save computation time, the model works with reduced magnitudes. This leads to a system of equations that are scale independent. Using the new system of equations, one can switch from physical variables to system variables. There are fewer system variables than physical variables, which considerably reduces the computation time when systematically scanning through all parameters that influence the system. Another effect of the switching from physical to system variables is to avoid unnecessary inaccuracy in the numerical calculations. The equations of motion were scaled using values that are characteristic for this system. These values are indicated by a zero subscript. In the equations below, the physical parameters with a tilde above them denote the respective variable without units.

$$\begin{aligned}
\frac{d\mathbf{r}}{dt} &= \frac{d(R_0\tilde{\mathbf{r}})}{d(t_0\tilde{t})}\\
&= \frac{1}{6\pi\eta R_0\tilde{R}}\frac{d}{d(R_0\tilde{\mathbf{r}})}(m_0\tilde{\mathbf{m}}B_0\tilde{\mathbf{B}}).
\end{aligned} \tag{15}$$

Using $B_0 = \frac{\mu_0 m_0}{R_0^3}$, this leads to:

$$\dot{\tilde{\mathbf{r}}} = \frac{\mu_0 t_0 m_0^2}{6\pi\eta R_0^6}\frac{1}{\tilde{R}}\tilde{\nabla}(\tilde{\mathbf{m}}\tilde{\mathbf{B}}), \tag{16}$$

and

$$\begin{aligned}
\frac{d\mathbf{e}}{dt} &= \frac{d\mathbf{e}}{d(t_0\tilde{t})}\\
&= -\frac{m_0\tilde{\mathbf{m}}}{8\pi\eta R_0^3\tilde{R}^3}B_0(\mathbf{e}(\mathbf{e}\tilde{\mathbf{B}}) - \tilde{\mathbf{B}})\\
\Rightarrow \dot{\tilde{\mathbf{e}}} &= -\frac{\mu_0 t_0 m_0^2}{8\pi\eta R_0^6}\frac{\tilde{\mathbf{m}}}{\tilde{R}^3}(\mathbf{e}(\mathbf{e}\tilde{\mathbf{B}}) - \tilde{\mathbf{B}}),
\end{aligned} \tag{17}$$

where μ_0 is the permeability of free space in SI units.

3.4 Brownian motion

According to Debye (1929), the relaxation time of a system of particles can be calculated using the formula:

$$\tau = \frac{\zeta}{2kT}, \tag{18}$$

where ζ is a constant satisfying

$$\mathbf{L} = -\zeta\dot{\varphi}. \tag{19}$$

In this case, $\mathbf{L}$ is the torque produced by the viscosity of the fluid and $\zeta = 8\pi\eta R^3$ for spherical particles.

Translational Brownian motion is accounted for by adding a random number drawn from a normal distribution with standard deviation $\sigma_x = \sqrt{\frac{kT2\Delta t}{6\pi\eta R_i}}$ (Joos 1959) to an existing particle position. For the rotation, an Euler pole is chosen from a uniform distribution across the surface of a sphere. A rotation matrix is constructed around this pole using an angle drawn from a normal distribution with standard deviation $\sigma_\theta = \sqrt{\frac{4kT\Delta t}{8\pi\eta R_i^3}}$ (Debye 1929). Again, these equations must be transformed to a reduced form as discussed in Section 3.3:

$$\tilde{\sigma}_x = \sqrt{\frac{2t_0kT}{6\pi\eta R_0^3}\frac{\Delta\tilde{t}}{\tilde{R}_i}}, \quad \text{and} \tag{20}$$

$$\tilde{\sigma}_\theta = \sqrt{\frac{4t_0kT}{8\pi\eta R_0^3}\frac{\Delta\tilde{t}}{\tilde{R}_i^3}}. \tag{21}$$

For axisymmetric particles the translation and rotational components of Brownian motion can be considered as acting independently of each other. In the case of irregularly shaped particles it would be necessary to couple the translational and rotational motions (Harvey & de la Torre 1980).

3.5 Numerical details of the model

Naturally occurring magnetic particles tend to form clusters as soon as they get close to each other. This is accounted for in the model by replacing two particles *i* and *j* that are less than twice the sum of their radii apart by a new particle:

$$|\mathbf{r}_i - \mathbf{r}_j| < 2(R_i + R_j).$$

The volume of the new particle is set as the sum of the two former volumes, while the magnetic moment is the vector sum of the two former moments.

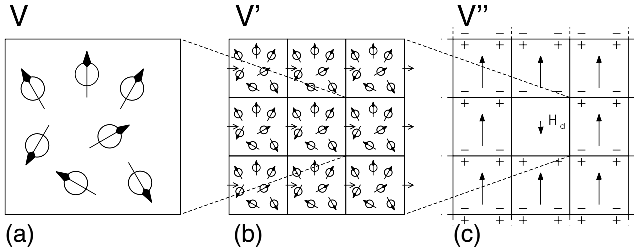

Figure 7. The n particles that are simulated are situated inside the centre box V of a cube V' consisting of 27 boxes. The other 26 boxes contain shifted images of the centre box. This should account for more realistic conditions while simulating the experiment, since the number of particles that can be handled at once is rather small. The large black arrows in (c) denote the average magnetization within each box. H_d is the demagnetizing field.

The numerical solver used to solve the differential equations is an adaptive Runge-Kutta solver (Press *et al.* 1992). It adjusts the magnitude of the time steps it takes according to the gradient of the function, thus ensuring that the dipoles will not oscillate around each other when one gets into the vicinity of the other.

For the calculations to be statistically representative, a large number of particles should be simulated. Since particle–particle interaction is taken into account, the computation time increases according to the square of the number of particles. Therefore, calculations dealing with many particles rapidly become cumbersome. In order to solve this problem, the computation space is assumed to be homogeneously magnetized. The space is split into 3 × 3 × 3 equally sized cubes, each holding the same particle subset. For the particles within the central box, the equations of motion are solved taking into account the magnetic fields of the particles within the box and the 26 surrounding boxes. The field due to all other particles is taken into account by introducing their demagnetizing field, again assuming homogenous magnetization (Fig. 7). This leads to the following equation for the magnetic field within V:

$$\mathbf{B}(\mathbf{r}) = \sum_{\mathbf{r}_i \in V'} \mathbf{B}(\mathbf{r}, \mathbf{r}_i, \mathbf{m}_i) + \mu_0 \mathbf{H}_d(\mathbf{r}). \tag{22}$$

The magnetostatic field in eq. (22) is obtained by calculating the surface charge potential Φ of the outer box, where its negative gradient is the demagnetizing field (Fabian *et al.* 1996):

$$\phi(\mathbf{r}) = \frac{1}{4\pi}\left[\int_V \frac{-\nabla\mathbf{M}(\mathbf{r}')}{|\mathbf{r}-\mathbf{r}'|}\,dV' + \int_S \frac{\mathbf{M}(\mathbf{r}')\cdot\mathbf{n}(\mathbf{r}')}{|\mathbf{r}-\mathbf{r}'|}\,dS'\right],$$

$$= \frac{1}{4\pi}\int_S \frac{\mathbf{M}(\mathbf{r}')\cdot\mathbf{n}(\mathbf{r}')}{|\mathbf{r}-\mathbf{r}'|}\,dS' \quad \text{and}$$

$$\mathbf{H}_d = -\mathrm{grad}\,\phi.$$

V and S are the sample volume and surface, respectively, and $\mathbf{n}$ is the outward surface normal. Since the magnetization $\mathbf{M}$ is treated as constant inside the boxes, $-\nabla\mathbf{M}$ equals zero. The magnetostatic field is also expressed as a reduced magnitude:

$$\mathbf{H}(\mathbf{r}) = \frac{m_0}{R_0^3}\tilde{\mathbf{H}}(\tilde{\mathbf{r}}).$$

In order to maintain energy and momentum within the computation space, we use periodic boundary conditions: a particle that leaves a box at one side re-enters at the opposite side. The numerical model runs start with all particles aligned in one direction. Since there is no external field, the particles immediately start to rearrange. The

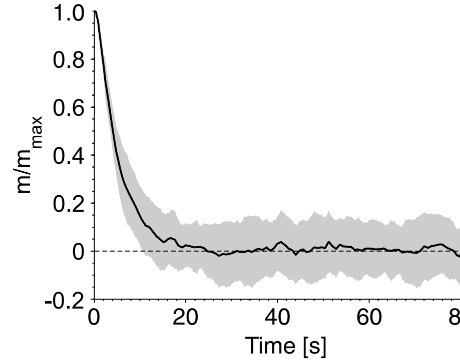

Figure 8. Individual runs of the numerical model consisting of 20 particles. For each configuration, 50 runs were calculated with the particles in different initial positions. The final decay curve for a given configuration was obtained by stacking the 50 runs (arithmetic mean, shown as the black line) and determining their standard deviation at each time point (shaded area). It can been seen that at some points the magnetization becomes negative, however, the magnitude of the negative value is substantially smaller than the standard deviation of the signal.

relaxation pattern of a system of 20 particles was observed as a function of the particle concentration and radii. For each radius and concentration combination, 50 model runs were stacked to produce a more representative data set, as shown in Fig. 8.

3.6 Model runs

To investigate what causes the three different relaxation patterns observed by Yoshida & Katsura (1985), magnetization was calculated as a function of scale length (R_0), scale length of magnetic moment (m_0) and particle concentration c, which is a substitute for $\tilde{\mathbf{R}}$. These three parameters are the only ones that need to be varied because they cover all possible configurations for the system parameters (*cf.* Section 3.3). The parameter space covered in the calculations is shown in Table 1. The chosen values correspond to those of naturally occurring magnetite samples. The reason for selecting a mineral with a large magnetic moment is to maximize the contribution from magnetostatic interactions.

3.7 Numerical results

The current state of the model quantitatively reproduces *Class 3* relaxation patterns as observed by Yoshida & Katsura (1985). The simulated data can be fitted using one exponential function and a constant:

$$f(t) = a_1 e^{-a_2 t} + a_3. \tag{23}$$

In cases where the magnetization was seen to pass through negative values, indicating the possibility of a *Class 2* decay, it was necessary

Table 1. Range of values for parameters used in the model.

Particle radius	0.1–10 μm
Magnetic moment	$4.27 \cdot 10^{-16} - 9.57 \cdot 10^{-11}$ A m^{-2}
Concentration	1/16–256 ppm
Number of particles	20
Number of stacked runs	50

Eight particle radii and eight magnetic moments equally distributed on a logarithmic scale, as well as 12 different concentrations equally distributed on a $\log_2$ scale, were chosen.

to test the significance of the negative feature in the curve. Initially, the mean equilibrium magnetization of the end of the decay curve was determined. This value was then compared to the mean value of the minimum of the curve using Student's *t*-test. The test was performed on the individual curves and it was found that no decay showed a significant polarity switch at the 0.05 level. Therefore, the polarity switches are simply a product of noise due to the relatively small particle assemblages employed in the model and none of the configurations produced a *Class 2* curve of the type reported by Yoshida & Katsura (1985).

It is reasonable to assume that if magnetostatic interactions are playing an important role, then a clear relationship should exist between the magnetic moment of the particles and the rate of magnetization decay. Using eq. (1) a prediction of the effective particle size, R_{eff}, was made for each decay curve. This value was compared to the input radius of the model to give the ratio R/R_{eff}. Thus, if magnetization decay occurs more rapidly than expected for a given input radius the ratio will have a value greater than 1. Box and Whisker plots are shown for the model runs with different magnetic moments (Fig. 9). There is a clear trend towards more rapid decay (ratio values >1) as the moment increases and this must be attributed to the effect of magnetostatic interaction. Interestingly, ratios <1 are found for the weakest moments, indicating a slower than expected decay. This property is anticipated if the magnetostatic interactions in the system are weak. When particles clump in the presence of strong interactions they will tend to rotate into orientations which cause mutual cancellation of their individual magnetizations, increasing the overall decay rate of the entire assemblage. When interactions are weak, less cancellation will occur during clumping, resulting in a movement towards slower decay rates due to the cluster's resistance to Brownian motion.

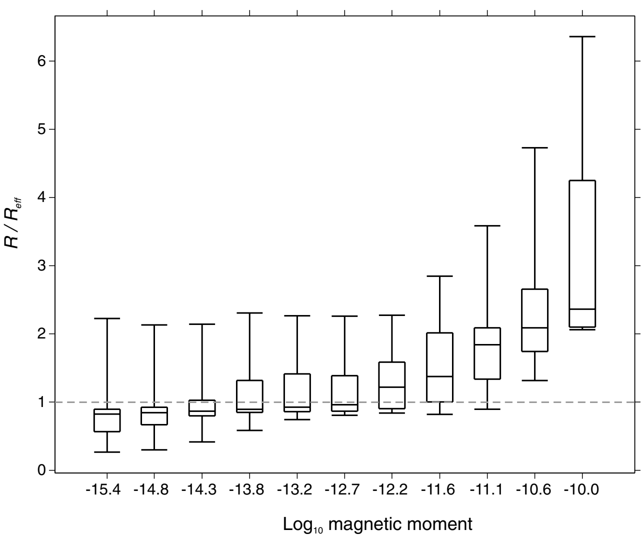

Figure 9. A box and whisker plot showing the distribution of R/R_{eff} as a function of particle magnetic moment. The lower and upper lines of the 'box' are the 25th and 75th percentiles of the sample. The distance between the top and bottom of the box is, therefore, the interquartile range. The line in the middle of the box is the sample median. If the median is not centred in the box, that is an indication of skewness. The 'whiskers' are lines extending above and below the box showing the extent of the rest of the results. The dashed grey line marks $R/R_{\mathrm{eff}} = 1$ which is where the model result is expected to occur for a suspension with no magnetostatic interactions and no particle–particle collisions. The clear shift to $R/R_{\mathrm{eff}} > 1$ for high particle moments demonstrates the effect of magnetostatic interactions increasing the magnetization decay rate.

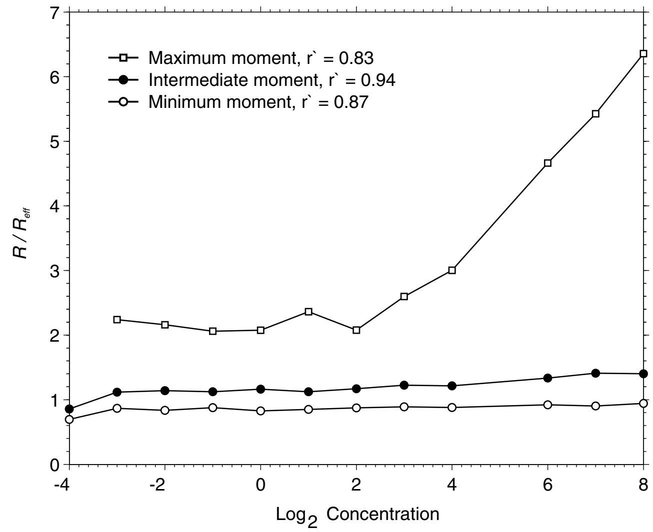

Figure 10. The ratio R/R_{eff} shows a significant monotonic increase, indicating increased magnetization decay rate, as a function of suspension concentration. The overall effect is slight in the systems with low and intermediate magnetic moments, demonstrating the weak effect of the magnetostatic interactions. In contrast, a strong effect is observed in the high moment system once a threshold concentration of 4 ppm is passed. The Spearman rank correlation coefficient of each line is give by r'.

From the experimental data presented in Fig. 6, we would also expect to see a relationship in the numerical results of greater interaction expressed as increasing values of R/R_{eff} as concentration is increased. R/R_{eff} is shown as a function of concentration for the models with the lowest, highest and an intermediate value of the magnetic moment (Fig. 10). Firstly, based on the Spearman rank correlation, all of the curves show a significant ($\alpha < 0.005$) monotonic increase in R/R_{eff}, indicating the greater importance of magnetostatic interactions as concentration increases. It is apparent that for the low and intermediate magnetic moments only a small effect on the magnetization is caused by increasing the concentration. In contrast, magnetization decay increases strongly in the high moment system at concentrations above 4 ppm.

The numerical models show that the magnetic moments of the particle assemblage have the greatest influence on the level of magnetostatic interaction, while concentration has a lesser, secondary effect. For the experimental investigation, the sediment suspensions produced from a single sediment should have identical distributions of particle magnetic moments. Therefore, it is necessary to study magnetostatic interactions within the suspensions solely as a function of concentration.

4 DISCUSSION

Both the laboratory results and the numerical models show more rapid decay rates as suspension concentration is increased. This pattern indicates that clumping, as a result of particle collisions due to Brownian motion or magnetostatic interactions, plays a key role in controlling magnetization decay. In an attempt to unify the laboratory and numerical results, the influence of clumping will be considered in detail.

Our numerical models produced magnetization decays that can be fitted with a function of the form given in eq. (23). As previously stated, if two model particles come into contact, they are replaced with a new particle with a volume based on the sum of their individual volumes. Therefore, in cases where particles clump, the coefficient a_2 corresponding to the relaxation time will not be constant with respect to time because of the particle size dependence of Brownian motion.

To investigate the effects of clumping, we compare the characteristic relaxation time for models with different initial particle concentrations. For a single model configuration, that is, constant initial radius and constant magnetic moment, we take the ratio of the number of magnetic particles remaining at the end of the c_8 (lowest concentration) and c_0 (highest concentration) runs. Thus, if increased concentration leads to increased particle clumping, the ratio n_{c_8}/n_{c_0} will be greater than unity.

To assess the rate of decay of the magnetization a characteristic time, t, is determined, corresponding to the period required for the magnetization to decay to half of its initial value. The particle ratio n_{c_8}/n_{c_0} is compared to the ratio of characteristic relaxation times for the c_8 and c_0 runs, t_{c_8}/t_{c_0} (Fig. 11). It is found that the majority of the model systems have a ratio n_{c_8}/n_{c_0} greater than unity, indicating that increases in concentration result in greater particle clumping. With respect to relaxation time, if particle clumping in the model was due solely to Brownian motion, then t_{c_8}/t_{c_0} would be expected to be less than unity as the effective particle size of the system increases with increasing concentration. The results of the numerical experiments show a monotonous increasing relationship in t_{c_8}/t_{c_0} with respect to n_{c_8}/n_{c_0}. This demonstrates that with increased clumping the system magnetization decays more rapidly. This pattern is the reverse to that expected if Brownian motion dominates the system and must, therefore, be attributed to the effects of magnetostatic interaction.

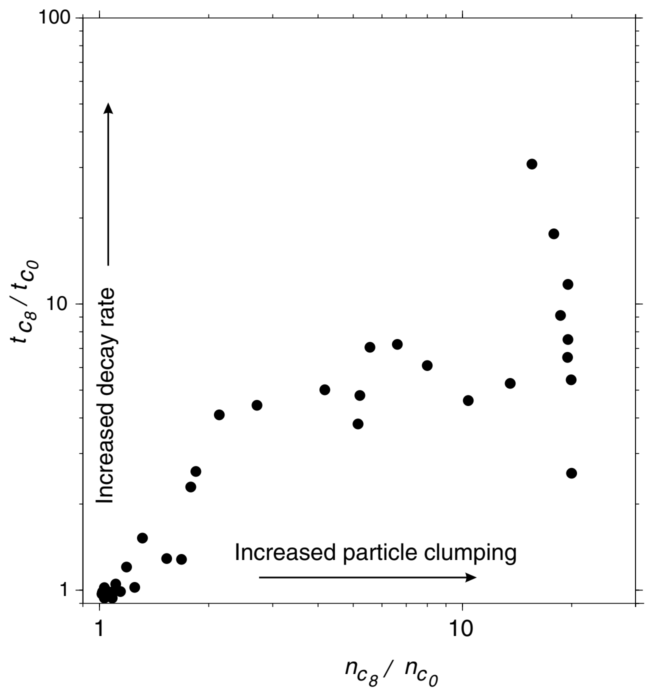

Figure 11. A number of the model systems demonstrate particle clumping, producing ratios of n_{c_8}/n_{c_0} (the number of particles remaining in the lowest concentration assemblage divided by the number of particles remaining in the highest concentration assemblage) greater than 1. Each simulation consisted of 20 particles, therefore, n_{c_8}/n_{c_0} can take a maximum value of 20. It is also apparent that the magnetization decay time for low-concentration assemblages is longer than for their high-concentration counterparts ($t_{c_8}/t_{c_0} > 1$). The monotonically increasing relationship between the particle and time ratios shows that increased suspension concentration results in greater particle clumping, which in turn reduces magnetization decay time.

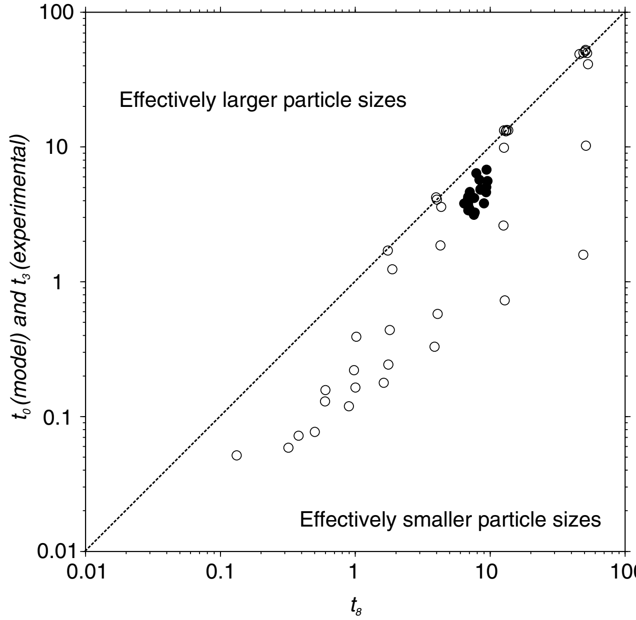

Figure 12. A comparison of the characteristic magnetization decay times for the numerical simulations (open symbols) reveals a difference in the effective particle size of low- and high-concentration systems. Points below the line of unity indicate a more rapid decay in the high-concentration system, demonstrating the effect of magnetostatic interactions. When plotted in the same space, the results of the laboratory experiments (closed symbols) show similar behaviour, which provides evidence for the presence of significant magnetostatic interactions in the prepared sediment suspensions.

The role of particle clumping in increasing the rate of magnetization decay is illustrated further in Fig. 12 where t_{c_0} is plotted against t_{c_8}. Where the system is dominated by Brownian motion and no particle clumping takes place, the points should plot along a line of unity. In cases where Brownian motion is responsible for particle clumping and magnetostatic interaction is negligible, the points should plot above the line of unity indicating a movement to larger effective particle sizes with increasing concentration. For the numerical experiments, all the points plot on or below the line of unity demonstrating the role of magnetostatic interactions. The experimental results obtained from the sediment suspensions are compared directly to the numerical results in Fig. 12. In a number of the sediment suspensions, *Class 1* curves were observed for the highest concentrations c_0 and c_1, therefore, the plotted data points are based upon a comparison between t_{c_3} and t_{c_8}. As with the numerical models all of the experimental data plot below the line of unity demonstrating the influence from magnetostatic interactions upon the magnetization decay. As discussed previously the viscosity of a suspension is expected to increase with increasing sedimentation concentration, reducing the effect of rotational Brownian motion. This effect is evident in the highest concentration suspensions, which act as slurries and produce *Class 1* type curves, however, Fig. 12 shows that t_{c_3} compared to t_{c_8} gives the reverse situation with low-concentration suspensions relaxing more slowly. This indicates that for the concentrations between c_3 and c_8 the viscosity differences between the suspensions do not play an important role in the relaxation behaviour.

Given the characteristic relaxation time of the experimental curves and working under an assumption of spherical particles it

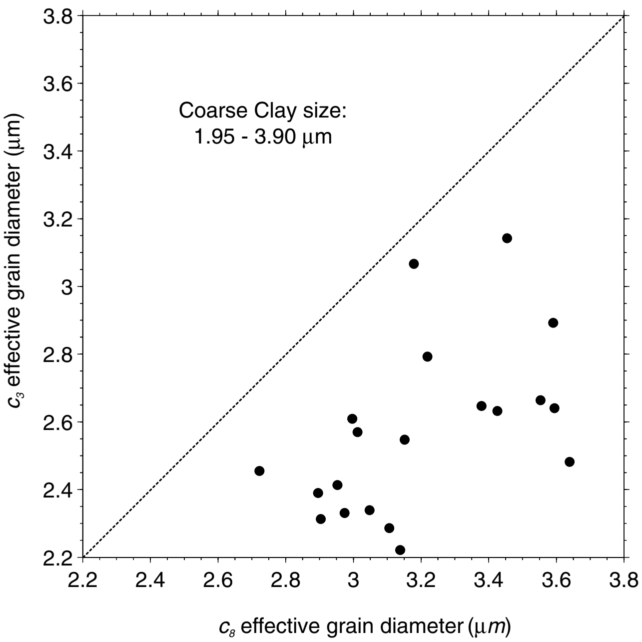

Figure 13. Using eq. (1) to determine effective particle size for the low c_8 and high c_3 concentration suspensions reveals that the small magnetic particles appear to be attached to larger sediment grains in the size range of coarse clay.

is possible to use eq. (1) to give an approximate size of the magnetic particles in each suspension (Fig. 13). As expected the low-concentration suspensions have larger effective grain sizes than their high-concentration counterparts. Interestingly the effective grain size for the suspensions is substantially larger than the single-domain size predicted by the hysteresis data. From the grain sizes predicted from the magnetization decay it is apparent that the magnetic particles are probably attached to larger clay particles, thus forming flocs that are more resistant to Brownian motion. The possibility of this effect has previously been discussed by Katari & Tauxe (2000), who proposed that magnetite particles would always be attached to larger clay grains and that this combination should be considered as the smallest unit in terms of DRM formation. The role of clumping between magnetic and nonmagnetic particles is clearly demonstrated by the occurrence of *Class 1* curves where the formation of an ordered fabric in the slurry resulted in little or no magnetization decay.

5 CONCLUSIONS

The reported laboratory and numerical results have revealed a number of important aspects concerning the magnetization behaviour of sediment suspensions. In the highest concentration cases the suspensions acted as slurries (Shcherbakov & Shcherbakova 1987), dramatically reducing grain mobility and forming a structure resistant to magnetization decay. This has important implications for DRM behaviour at the sediment–water interface. The ability of a magnetic grain to reorient must be reduced substantially even within the highly porous fabric at the sediment surface.

Unification of the laboratory and numerical results has revealed that magnetization decay in suspensions is at least partially a function of concentration. It is apparent that particle clumping plays a key role in controlling the magnetization decay behaviour of the suspension. As concentration increases it was found that magnetization decayed more rapidly. This provides evidence for the influence of magnetostatic interactions, which tend to clump magnetic particles together in orientations that will cause cancellation of their magnetization vectors. Such a relationship between concentration and decay rate cannot be explained by changes in suspension viscosity or the effect of Brownian motion on particle clumps. Considering the work of Yoshida & Katsura (1985), neither our experimental results nor our numerical model reproduce *Class 2* relaxation patterns as observed in their studies even though we have evidence for the occurrence of significant magnetostatic interactions. It is, therefore, apparent that processes other than Brownian motion and magnetostatic interactions may have be responsible for the magnetization reversals observed in the sediment suspensions of Yoshida & Katsura (1985).

Hysteresis parameters of the studied sediments indicate that the magnetic assemblage is predominantly in the stable single-domain grain size range. In contrast, analysis of the sediment suspension characteristic decay times in terms of Brownian motion has revealed a substantially slower magnetization decay than would be expected for single-domain particles. It is found that the effective size of the magnetic particles is between 2.2 and 3.8 μm and, therefore, in the coarse clay range. This finding supports the hypothesis of Katari & Tauxe (2000) that the majority of sedimentary magnetite particles will be attached to larger clay particles and that this combination should be considered as the smallest unit in DRM studies.

ACKNOWLEDGMENTS

We wish to thank Andrew Roberts and Valera Shcherbakov for detailed reviews that substantially improved the manuscript. This work was funded by the DFG priority program 'Geomagnetic Variations' and by the DFG Research Centre 'Ocean Margins' of the University of Bremen.

REFERENCES

Anson, G.L. & Kodama, K.P., 1987. Compaction-induced inclination shallowing of the postdepositional remanent magnetization in a synthetic sediment., *Geophys. J. R. astr. Soc.,* **88,** 673–692.

Barton, C.E., McElhinny, M.W. & Edwards, D.J., 1980. Laboratory studies of depositional DRM, *Geophys. J. R. astr. Soc.,* **61,** 355–377.

Bennett, R.H., O'Brien, N.R. & Hulbert, M.H., 1991. Determinants of clay and shale microfabric signatures: Processes and mechanisms, in *Microstructure of Fine-Grained Sediments, From Mud to Shale*, pp. 5–32, eds Bennett, R.H., Bryant, W.R. & Hulbert, M.H., Springer-Verlag New York.

Collinson, D.W., 1965. Depositional remanent magnetization in sediments, *J. geophys. Res.,* **70,** 4663–4668.

Currie, I.G., 2002. *Fundamental Mechanics of Fluids*, Marcel Dekker Ltd., New York.

Debye, P., 1929. *Polare Molekeln*, Leipzig: Hirzel.

Dormy, E., Valet, J.-P. & Courtillot, V., 2000. Numerical models of the geodynamo and observational constraints, *Geophys. Geochem. Geosyst.,* **1,** 1–42.

Fabian, K., Kirchner, A., Williams, W., Heider, F., Leibl, T. & Hubert, A., 1996. Three-dimensional micromagnetic calculations for magnetite using FFT, *Geophys. J. Int.,* **124,** 89–104.

Fannin, P.C., Charles, S.W. & Relihan, T., 1995. On the influence of inertial effects, arising from rotational Brownian motion, on the complex susceptibility of ferrofluids, *J. Phys. D: Appl. Phys.,* **28,** 1765–1769.

Franke, C., Hofmann, D. & von Dobeneck, T., 2004. Does lithology influence relative paleointensity records? A statistical analysis on South Atlantic pelagic sediments, *Phys. Earth planet. Inter.,* **147,** 285–296.

Fukuma, K., 1992. A numerical simulation of magnetic coagulation in a fluid, *Geophys. J. Int.,* **111,** 357–362.

Gerthsen, C. & Vogel, H., 1993. *Physik*, Springer-Verlag, Heidelberg.

Griffiths, D., King, R., Rees, A. & Wright, A., 1960. Remanent magnetism of some recent varved sediments, *Proc. Roy. Soc. London, Ser. A,* **256,** 359–383.

Guyodo, Y., Gaillot, P. & Channell, J.E.T., 2000. Wavelet analysis of relative geomagnetic paleointensity at ODP site 983, *Earth planet. Sci. Lett.,* **184,** 109–123.

Harvey, S.C. & de la Torre, J.G., 1980. Coordinate systems for modeling the hydrodynamic resistance and diffusion coefficients of irregularly shaped rigid macromolecules, *Macromolecules,* **13,** 960–964.

Irving, E. & Major, A., 1964. Post-depositional detrital remanent magnetization in a synthetic sediment, *Sedimentology,* **3,** 135–143.

Joos, G., 1959. *Lehrbuch der theoretischen Physik*, Akademische Verlagsgesellschaft M.B.H. Frankfurt am Main.

Katari, K. & Bloxham, J., 2001. Effects of sediment aggregate size on DRM intensity: a new theory, *Earth planet. Sci. Lett.,* **186,** 113–122.

Katari, K. & Tauxe, L., 2000. Effects of pH and salinity on the intensity of magnetization in redeposited sediments, *Earth planet. Sci. Lett.,* **181,** 489–496.

Kent, D.V., 1973. Post depositional remanent magnetization in deep sea sediments, *Nature,* **246,** 32–34.

King, R.F. & Rees, A.I., 1966. Detrital magnetism in sediments: an examination of some theoretical models, *J. geophys. Res.,* **71,** 561–571.

Kono, M. & Roberts, P., 2002. Recent geodynamo simulations and observations of the geomagnetic field, *Rev. Geophys.,* **40,** 1–53.

Kranck, K., 1991. Interparticle grain size relationships resulting from flocculation, in *Microstructure of Fine-Grained Sediments, From Mud to Shale*, pp. 125–130, eds Bennett, R.H., Bryant, W.R. & Hulbert, M.H., Springer-Verlag New York.

Langereis, C., Dekkers, M., de Lange, G., Paterne, M. & van Santvoort, P., 1997. Magnetostratigraphy and astronomical calibration of the last 1.1 myr from an eastern Mediterranean piston core and dating of short events in the brunhes, *Geophys. J. Int.,* **129,** 75–94.

Løvlie, R., 1989. Magnetization of sediments and depositional environment, in *Geomagnetism and Palaeomagnetism*, pp. 243–252, ed. Lowes, F.J., Kluwer Academic Publishers, Norwell, MA.

Lu, R., Banerjee, S. & Marvin, J., 1990. Effects of clay mineralogy and the electrical conductivity of water on the acquisition of depositional remanent magnetization in sediments, *J. geophys. Res.,* **95,** 4531—4538.

Press, W.H., Flannery, B.P., Teukolsky, S.A. & Vetterling, W.T., 1992. *Numerical Recipes in C: The Art of Scientific Computing*, Cambridge University Press, Cambridge, UK.

Rees, A., 1961. The effect of water currents on the magnetic remanence and anisotropy of susceptibility of some sediments, *Geophys. J.,* **5,** 235–251.

Roberts, A.P. & Weaver, R., 2005. Multiple mechanisms of remagnetization involving sedimentary greigite (Fe_3S_4), *Earth planet. Sci. Lett.,* **231,** 263–277.

Roberts, A.P. & Winklhofer, M., 2004. Why are geomagnetic excursions not always recorded in sediments? Constraints from post-depositional remanent magnetization lock-in modelling, *Earth planet. Sci. Lett.,* **227,** 345–359.

Roberts, A.P., Pike, C.R. & Verosub, K.L., 2000. First-order reversal curve diagrams: a new tool for characterizing the magnetic properties of natural samples, *J. geophys. Res.,* **105,** 28 461–28 475.

Shcherbakov, V. & Shcherbakova, V., 1983. On the theory of depositional remanent magnetization in sedimentary rocks, *Geophys. Surv.,* **5,** 369–380.

Shcherbakov, V.P. & Shcherbakova, V.V., 1987. On the physics of post-depositional remanent magnetization, *Phys. Earth planet. Inter.,* **46,** 64–70.

Stacey, F.D., 1972. On the role of Brownian motion in the control of detrital remanent magnetization, *Pure appl. Geophys.,* **98,** 139–145.

Tauxe, L., 1993. Sedimentary records of relative paleointensity: theory and practice, *Rev. Geophys.,* **31,** 319–354.

Tauxe, L. & Kent, D.V., 1984. Properties of detrital remanence carried by hematite from study of modern river deposits and laboratory redeposition experiments, *Geophys. J. R. astr. Soc.,* **77,** 543–561.

Tauxe, L., Bertram, N. & Seberino, C., 2002. Physical interpretation of hysteresis loops: micromagnetic modeling of fine particle magnetite, *Geophys. Geochem. Geosyst.,* **3,** 1055, doi:10.1029/2001GC000241.

Truckenbrodt, E., 1980. *Fluidmechanik*, Vol. 1, Springer Verlag, Berlin.

Valet, J.-P., 2003. Time variations in geomagnetic intensity, *Rev. Geophys.,* **41,** 1–44.

Valet, J.-P., Meynadier, L. & Guyodo, Y., 2005. Geomagnetic dipole strength and reversal rate over the past two million years, *Nature,* **435,** 802–805.

van Vreumingen, M.J., 1993a. The magnetization intensity of some artificial suspensions while flocculating in a magnetic field, *Geophys. J. Int.,* **114,** 601–606.

van Vreumingen, M.J., 1993b. The influence of salinity and flocculation upon the acquisition of remanent magnetization in some artificial sediments, *Geophys. J. Int.,* **114,** 607–614.

Verosub, K.L., 1977. Depositional and postdepositional processes in the magnetization of sediments, *Rev. Geophys. Space Phys.,* **15,** 129–143.

Wartel, S., Singh, S. & Faas, R., 1991. The nature and significance of gas-generated microvoids as secondary microfabric features in modern and pleistocene marine and estuarine sediments, in *Microstructure of Fine-Grained Sediments, From Mud to Shale*, pp. 55–60, eds Bennett, R.H., Bryant, W.R. & Hulbert, M.H., Springer-Verlag, New York.

Yoshida, S. & Katsura, I., 1985. Characterization of fine magnetic grains in sediments by the suspension method, *Geophys. J. R. astr. Soc.,* **82,** 301–317.